AD-A081 861 NORTHROP CORP DES PLAINES IL DEFENSE SYSTEMS DIV F/G 9/5
I/J BAND LOW-COST CROSSED-FIELD AMPLIFIER.(U)
FEB 80 R R MOATS DAAB07-78-C-2981
UNCLASSIFIED 094-009246 DELET-TR-78-2981-2 NL

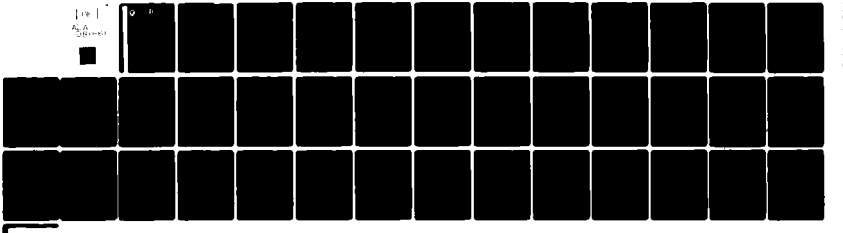

END
DATE FILMED
4-80
DTIC

LEVEL II

(1 of 2)

Research and Development Technical Report

DELET-TR-78-2981-2

I/J BAND LOW-COST CROSSED-FIELD AMPLIFIER

Robert R. Moats
NORTHROP DEFENSE SYSTEMS DIVISION
Electron Tube Section
Des Plaines, IL 60018

FEBRUARY 1980

Second Interim Report for Period 31 MARCH 1979 To 30 SEPTEMBER 1979

DISTRIBUTION STATEMENT
Approved for public release:
distribution unlimited

Prepared for: ELECTRONICS TECHNOLOGY & DEVICES LABORATORY

ERADCOM
US ARMY ELECTRONICS RESEARCH AND DEVELOPMENT COMMAND
FORT MONMOUTH, NEW JERSEY 07703

NOTICES

Disclaimers

The citation of trade names and names of manufacturers in this report is not to be construed as official Government indorsement or approval of commercial products or services referenced herein.

Disposition

Destroy this report when it is no longer needed. Do not return it to the originator.

SECURITY CLASSIFICATION OF THIS PAGE (When Data Entered)

REPORT DOCUMENTATION PAGE

READ INSTRUCTIONS BEFORE COMPLETING FORM

1. REPORT NUMBER: DELET-TR-78-2981-2	2. GOVT ACCESSION NO.
3. RECIPIENT'S CATALOG NUMBER	
4. TITLE (and Subtitle): I/J BAND LOW-COST CROSSED-FIELD AMPLIFIER	5. TYPE OF REPORT & PERIOD COVERED: Interim Technical Report, 31 March — 30 Sept 1979
6. PERFORMING ORG. REPORT NUMBER: 094-009246	
7. AUTHOR(s): Robert R. Moats	8. CONTRACT OR GRANT NUMBER(s): DAAB07-78-C-2981
9. PERFORMING ORGANIZATION NAME AND ADDRESS: Northrop Defense Systems Division, Electron Tube Section, 175 W. Oakton Street, Des Plaines, IL 60018	10. PROGRAM ELEMENT, PROJECT, TASK AREA & WORK UNIT NUMBERS: 1L162705AH94 01 M1
11. CONTROLLING OFFICE NAME AND ADDRESS: U.S. Army Electronics Research & Development Command - ATTN: DELET-BM, Fort Monmouth, NJ 07703	12. REPORT DATE: February 1980
	13. NUMBER OF PAGES: 38
14. MONITORING AGENCY NAME & ADDRESS (if different from Controlling Office)	15. SECURITY CLASS. (of this report): Unclassified
	15a. DECLASSIFICATION/DOWNGRADING SCHEDULE

16. DISTRIBUTION STATEMENT (of this Report)

Approved for Public Release - Distribution Unlimited

17. DISTRIBUTION STATEMENT (of the abstract entered in Block 20, if different from Report)

18. SUPPLEMENTARY NOTES

Prepared for : U.S. ARMY ELECTRONICS RESEARCH AND DEVELOPMENT COMMAND
FORT MONMOUTH, NJ 07703

19. KEY WORDS (Continue on reverse side if necessary and identify by block number)

Electron Tubes, Microwave Amplifiers, Crossed-Field Tubes, Shaped Substrate Meander Line, Laser Cutting

20. ABSTRACT (Continue on reverse side if necessary and identify by block number)

This program is directed toward development of an I/J band, linear format, injected-beam crossed-field amplifier (IBCFA) for electronic warfare. The IBCFA should be capable of power output of 1000W peak, 200W average, between 8.5 and 17GHz with 20dB gain. A laser-cut shaped-substrate meander line is used.

DD FORM 1 JAN 73 1473 EDITION OF 1 NOV 65 IS OBSOLETE

SECURITY CLASSIFICATION OF THIS PAGE (When Data Entered)

407171

The performance objectives for E/F band CFA's include 3kW peak pulse power output and 1kW average power output, 20dB gain, 2-4GHz, for electronic warfare; and 2kW peak pulse power output at 10-15% duty, 25dB gain, 3.0 to 3.6GHz, for phased-array radar. One E/F band tube has been built. Preliminary tests at 10% duty directed toward electronic warfare applications showed 3kW peak power at mid-band, 1.5kW at 2GHz, and 2.4kW at 4GHz. Increased drive power leads to greater power output at the low end of the band, indicating the need for greater circuit length. This tube will be tested further for its characteristics in the phased array mode and for full rated duty in the electronic warfare mode. Another E/F band tube is under construction, this one with increased circuit length.

Further large-signal calculations for the I/J band tube were performed directed toward the objectives, and final design parameters for the first operating tubes were chosen. Parts are now being fabricated.

A second cold-test model of an earlier design was build and tested. Measured values of delay ratio were in reasonable agreement with values calculated. Attenuation was also in reasonable agreement with calculations but only after a meander strip 0.003" thick was added to the meander strip etched from the metallizing. Further cold-test models similar in configuration to the operating tube design are under construction.

TABLE OF CONTENTS

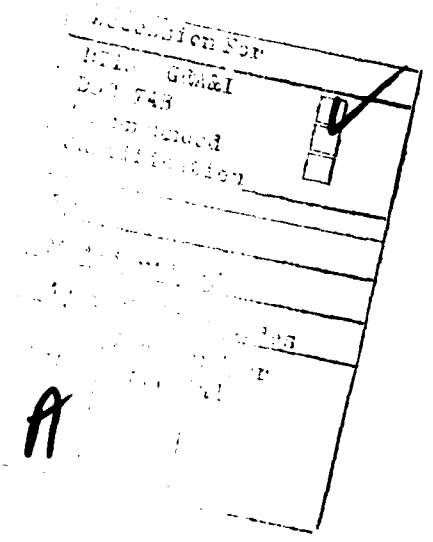

LIST OF ILLUSTRATIONS

SECTION I

INTRODUCTION

The effort in this program is directed toward the development of a high-power broad-band low-cost I/J-band linear format crossed-field amplifier (CFA) for electronic warfare. A laser-cut shaped-substrate meander line circuit is used. In addition, E/F-band CFA's of similar construction are to be built which can be applied either to electronic warfare or phased-array radar.

The laser-cut shaped-substrate meander circuit, a concept originated by ERADCOM personnel, is potentially a major cost saving measure, replacing a set of 80 or more individual insulators with a single part. Furthermore, the individual insulators for I/J-band would be so small as to be impractical.

The objective specifications for the E/F-band operating model for electronic warfare are as follows:

Frequency	2-4 GHz
Peak Power Output	3 kW
Average Power Output	1 kW
Efficiency	35%
Gain	20 dB
Cathode Voltage	7 kV
RF Input Impedance	50 ohms.

The phased-array objectives are as follows:

Frequency Range	3.0-3.6 GHz
Peak Power Output	2 kW
Duty	10 - 15%
Pulse Duration Capability with Grid Pulsing	100 μsec
Grid Cutoff Voltage	1 kV max
Efficiency (incl. heater)	30%
Gain	23 dB min
Line-to-sole Voltage	10 kV max
In-Band Power Variation	± 0.5 dB
Input/Output Connectors	Coaxial
Production Cost Objective	$1,000 max.

The performance objectives for I/J-band are as follows:

Frequency Range	8.5 - 17 GHz
Peak Power Output	1 kW
Average Power Output	200 W
Efficiency	30%
Gain	20 dB
Cathode Voltage	8 kV, max
Input Impedance	50 ohms

In a previous program for ERADCOM, operating E/F-band CFA's were built which have demonstrated the effectiveness of the laser-cut shaped substrate principle [1]. Performance was comparable with standard E/F-band CFA's. During the course of the present contract, one additional operating E/F-band CFA has been built and tested with similar results, and another, with a longer circuit, is under construction.

Additional I/J-band cold-test models have been built and tested. Attenuation represents the most critical parameter. Calculations indicate that acceptable attenuation can be achieved, but test results are ambiguous above 12 GHz. An improved cold-test model is under construction. Parts for an operating tube are being fabricated, with the design determined from calculations.

SECTION II

E/F-BAND TUBES

The first E/F-band CFA in this program has been built, using the same length circuit as those previously built. Initial tests for the electronic warfare mode (1.5 A peak be ٦ current) show substantially the same power output and efficiency at mid-band as the first CFA with a laser-cut substrate. At the high frequency end of the band power output and efficiency are better, and they are not as good at the low-frequency end of the band. Performance across the band under these conditions and at 10% duty are shown in Figure 1. From 2 to 2.6 GHz, power output is strongly dependent on RF drive power, indicating that a longer circuit is desirable. Power output as a function of RF drive in this frequency range is shown in Figure 2.

A second E/F-band CFA, designed for a circuit length six bars greater than before, is under construction. Assembly can be completed as soon as laser cutting of substrates has been completed.

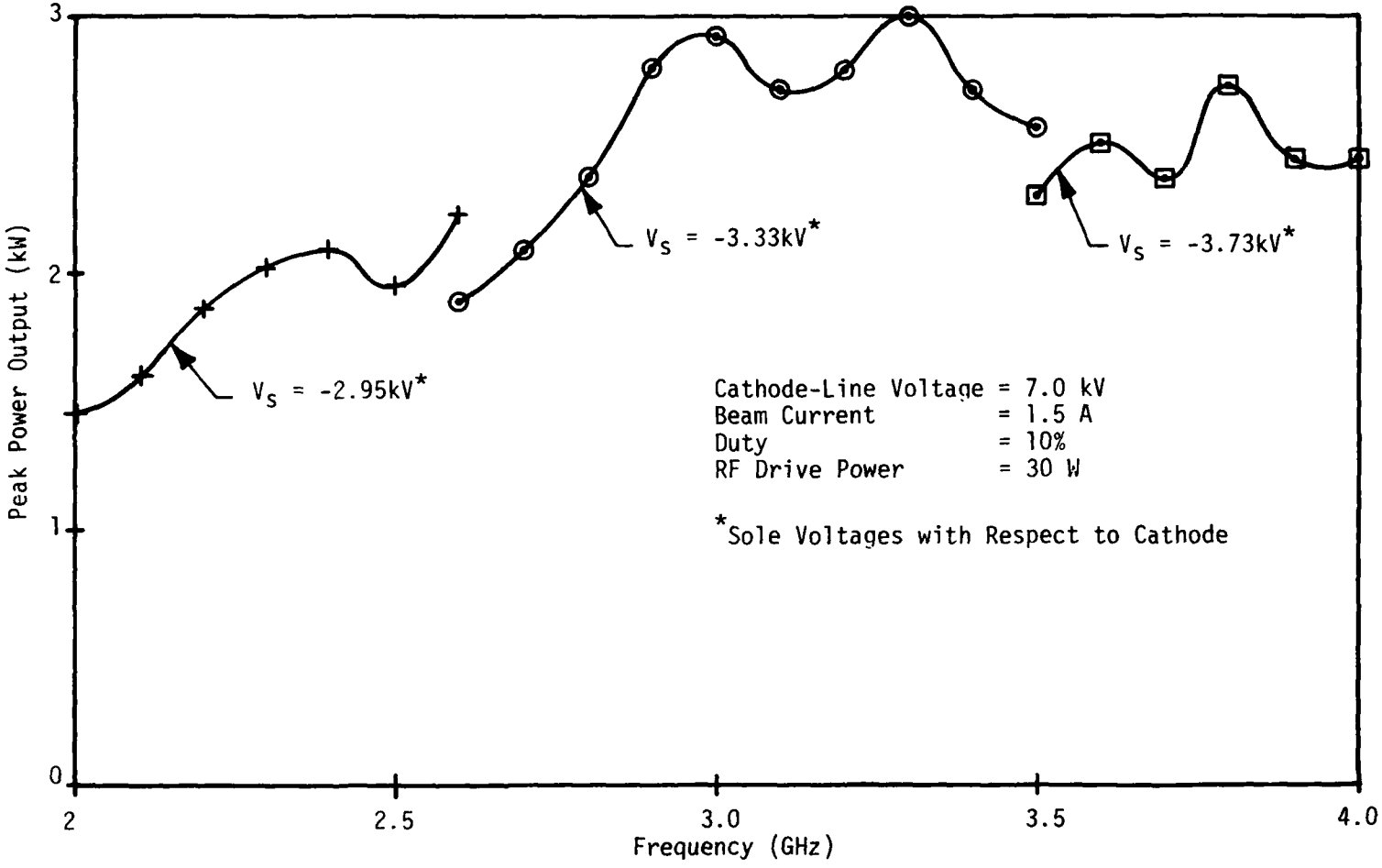

Figure 1. Power Output vs. Frequency, E/F Band CFA

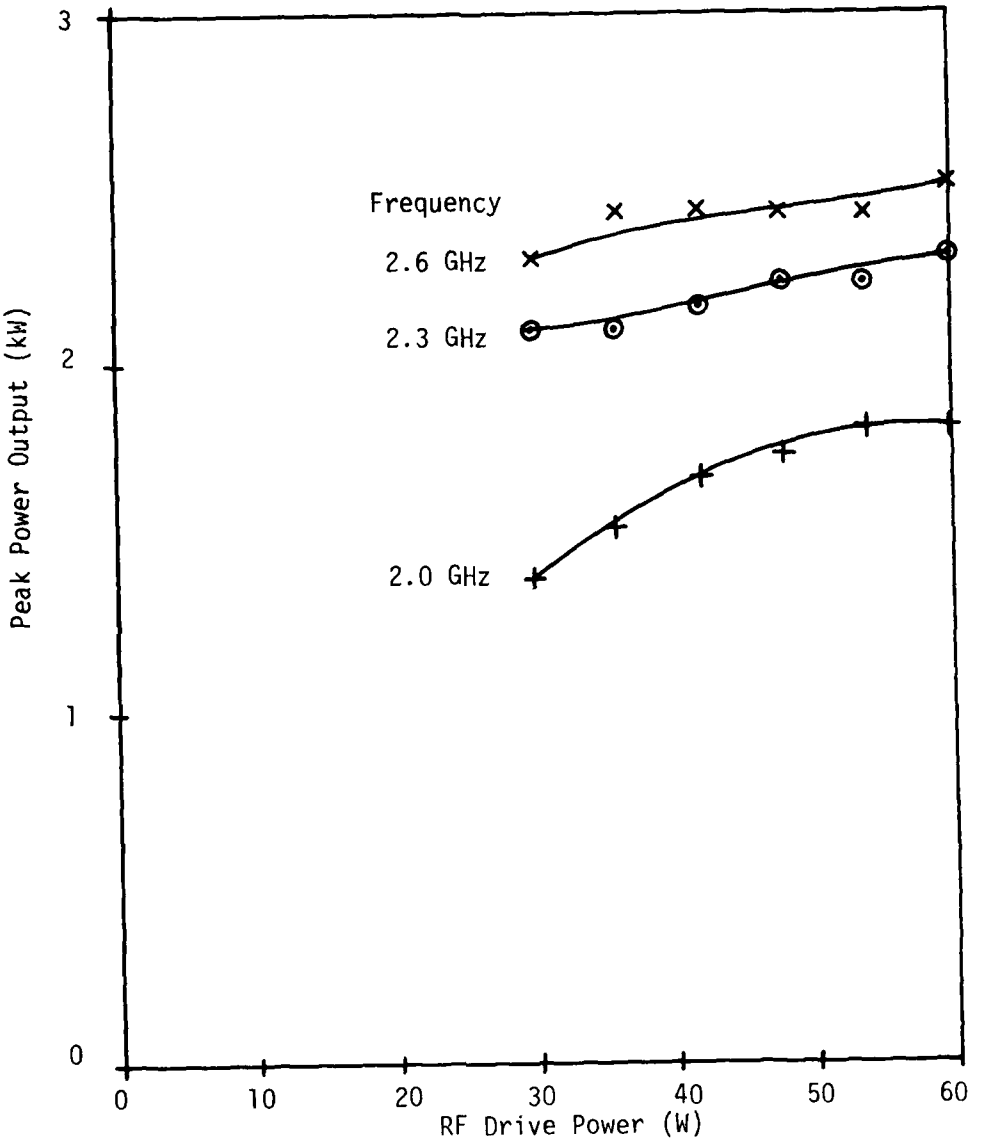

Figure 2. Power Output vs. RF Drive, E/F Band CFA

SECTION III

I/J-BAND TUBES

3.1 Design Calculations

Another series of large-signal calculations was made. These calculations were confined to values of pitch of 0.014" and 0.016". As an additional modification to the computer program, it was attempted to take into account the injection of a cycloiding beam instead of a rectilinear beam. In actual operating CFA's, the small-signal gain measured is greater than that calculated. If there is cycloiding, the centroid of the beam is closer to the circuit, the effective coupling impedance at the level of the beam is therefore greater, and the small signal gain is greater. Calculated results showed less small-signal gain with cycloiding than without. Further study of the mathematical model is needed. A final design for the I/J band operating models has been determined based on the large-signal calculations without cycloiding. The length of the circuit was reduced arbitrarily from 1.8 incnes to 1.5 inches based on experience. The pitch is to be 0.014" on a substrate thickness of 0.006", as previously contemplated.

3.2 I/J-Band Circuits

Another cold-test circuit was built to the same design as the previous cold-test circuit (0.018" pitch, 0.006" substrate thickness). Although the substrate was cracked at the center, results for this model were much improved.

The first set of tests was made with the meander circuit consisting only of the metallized layer. Because of the crack in the substrate only about half of the 50 bars were useful in the tests, and little meaningful test results could be taken above 12 GHz.

A photo-etched meander 0.003" thick was then bonded to the substrate and measurements repeated. It was now possible to measure phase velocity to above 17 GHz. Attenuation measurements were still limited to the region below 12 GHz.

Results of phase velocity measurement with and without the 0.003" add-on meander are shown in Figure 3. Also shown are calculated phase velocity measurements for both cases. The method of calculation is described in the Appendix.

As to attenuation, the values measured by resonance for the thin meander circuit between 8 and 12 GHz are about 0.5 dB per delayed wavelength, as compared with calculated values in the range of 0.33-0.27 dB per delayed wavelength from 8 to 12 GHz. For the circuit with the add-on meander the measured values are in the range of 0.34 to 0.38 dB per delayed wavelength, as compared with calculated values of 0.37 to 0.33 dB per delayed wavelength going from 8 to 12 GHz.

The calculations indicate that progressively thinner circuits correspond to less attenuation, limited only by the assumption that the circuit thickness is several times the skin depth. Numerical results for the thick (i.e., 0.003") I/J-band meander circuits are comparable with observed values. The calculations do not explain the much higher values of attenuation observed when the meander consists of the metallized layer only. The skin depth in copper at 10 GHz is 0.66 μm, and the nominal thickness of copper is 6 μm. Roughness at the edges of the meander as a result of the photo-etching is suspected to contribute to the excess losses.

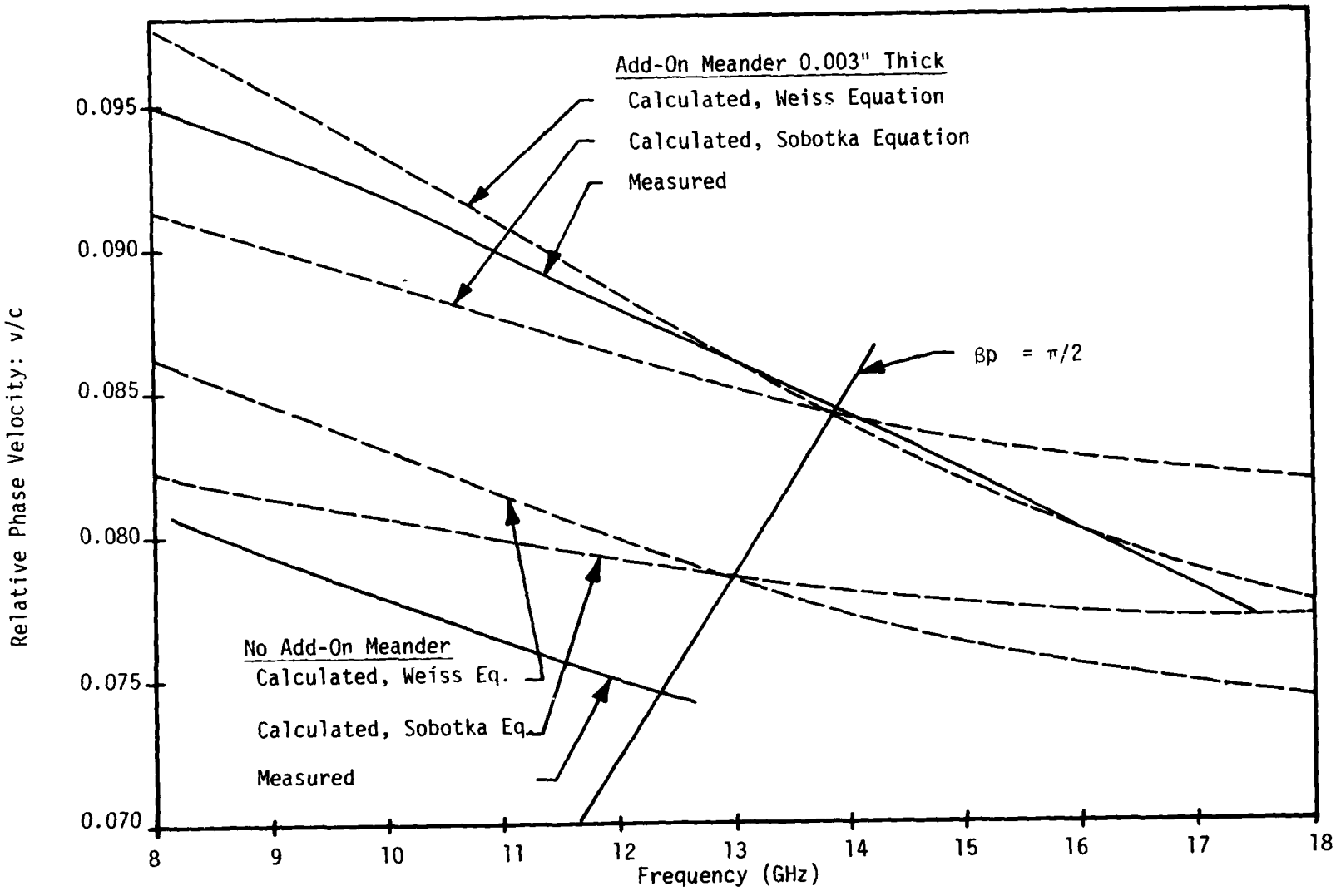

Figure 3. Phase Velocity, I/J Band Cold-Test Circuit

The next series of cold-test circuits is still under construction. Some serious delays were encountered due to reasons which were not fundamental to the new technology. First there were delays due to malfunctioning of the sputtering equipment. In one lot of three metallized coupons sent out for etching meander patterns, all three were broken during the process. One lot of coupons etched in house failed because the copper layer which was depended upon to resist the etchant used to remove Molybdenum also eroded the copper excessively. One coupon etched successfully in house was broken by a vendor in dicing the coupon into individual substrates. Another coupon etched in house had a corner broken off; there was enough remaining of this coupon that four usable substrates were diced from it. It is significant that in every case of breakage mentioned above, the same vendor or in-house organization performed the same operation previously and subsequently with success. Greater care and in some cases better handling procedures are required and are being implemented. The problems are not fundamental and do not involve the operation considered most critical, the laser cutting.

The sequence of fabricating the meander circuit has been reviewed once more. The process of attaching the add-on photo-etched meander after laser cutting has not been altogether satisfactory because of the flimsiness of that part. Two new options have been considered:

(1) Achieve a thicker copper layer on the substrate before photo-etching so that the add-on meander is unnecessary.

(2) Build up the meander thickness by electroforming with photo-resist in place.

The first of these two options requires only one photo-etching procedure, thus leading to simplification and cost reduction. One approach to realizing the thicker copper layer is to bond on a layer of foil by the same diffusion-bonding process now used to attach the add-on meander. An experiment was performed in which such a layer of foil 0.002" thick was bonded to a metallized BeO ceramic substrate 2" x 0.75" x 0.022" thick, and it was etched to form a strip 0.008" wide and about 0.722" long. A 60 Hz current of about 10 A was passed through this strip, with the opposite side of the substrate bearing on a cold plate. The temperature of the copper strip was measured, and the temperature rise was found to be close to calculated value in terms of the thickness of the ceramic. Therefore the bonding was considered satisfactory. A disadvantage of this approach is that etching is possible from only one side, and undercutting is therefore greater than in the case of the add-on meanders which may be etched from both sides. This disadvantage is not serious if the meander can be 0.001" thick or less. In this particular case undercutting due to etching was not serious.

The procedure of building up the meander by plating with photo-resist in place would overcome the problem of undercutting. However it is necessary either to perform two photo-masking operations, one after metallizing to form a thin meander, or to remove the metallization between meander bars by a light etch after the meander has been built up. In the latter case, one depends on the fact that the built-up meander is thick enough that it is not significantly damaged by the etching. A previous I/J-band meander

circuit was subjected to etching to remove unwanted metallizing after the add-on meander had been bonded to the substrate. The resulting circuit had greatly increased RF losses for reasons not yet understood. Therefore the photo-forming approach is not now being pursued.

Meanwhile the photo-etched add-on meander has been redesigned to incorporate two webs instead of one between successive segments to stiffen it.

3.3 Input/Output Windows

A coaxial window design suitable for the required output power level at frequencies up to 18 GHz has been designed. The frequency limitation depends primarily on the TM_{01} mode, which is excited by the step on the center conductor necessary for impedance matching. If this mode is cut off, the effect of the TM_{01} mode is a localized capacitance which may be easily compensated for. If this mode can propagate, a serious mismatch occurs. For the previously tested window designed for an X-band radar CFA the calculated TM_{01} cut-off occurs at about 14.5 GHz, which is close to its measured upper limit for good matching. In the new design, the calculated TM_{01} cut-off occurs at 18.2 GHz. An unbrazed coaxial window of this design was constructed using synthetic dielectric material instead of BeO ceramic. Maximum VSWR between 2 and 18 GHz was 1.2 as shown in Figure 4. Parts for brazed windows for operating tubes have been ordered.

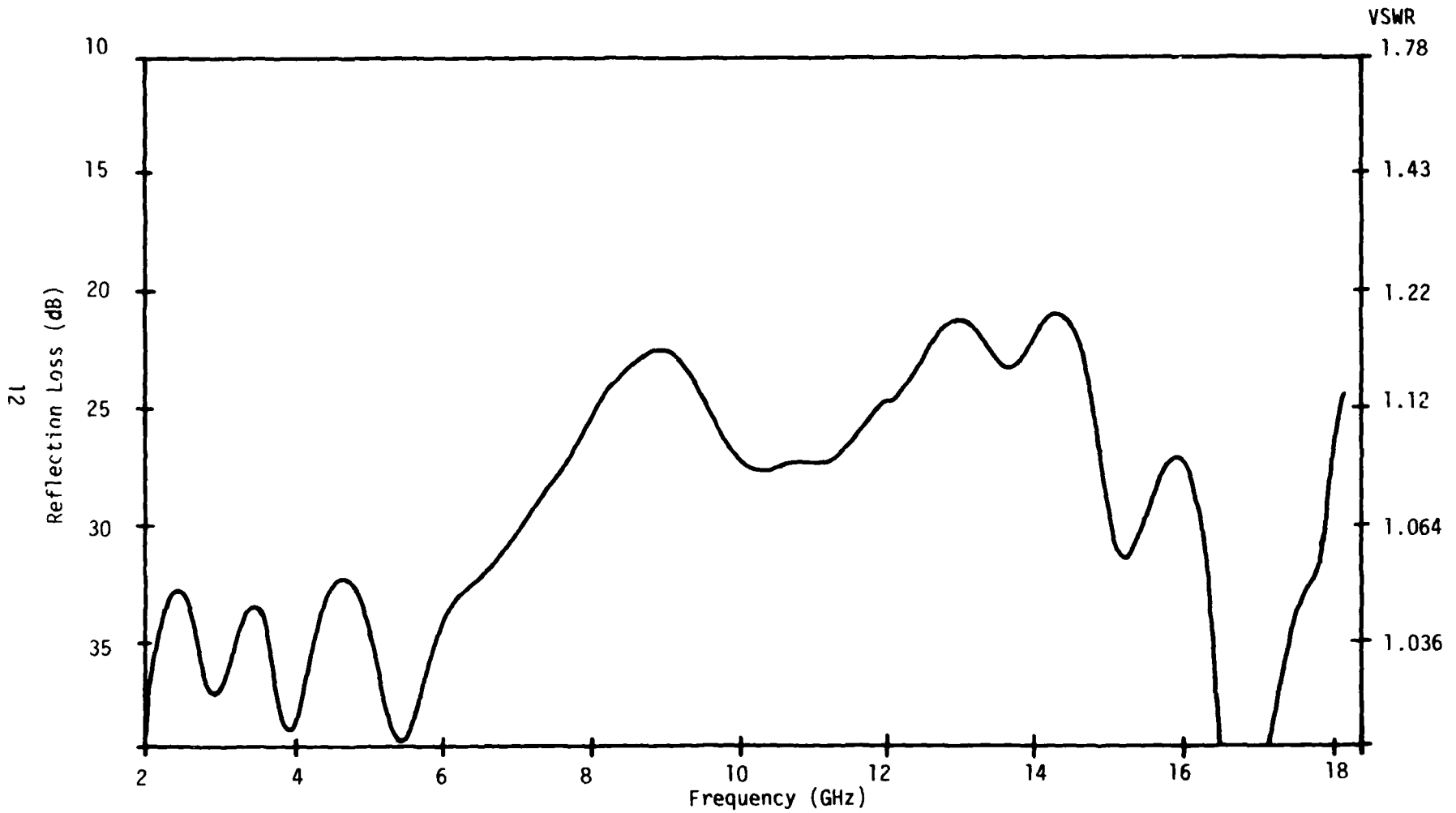

Figure 4. Matching of coaxial window with synthetic dielectric

SECTION IV

FURTHER WORK TO BE PERFORMED

4.1 E/F-Band CFA's

The most recently built E/F-band CFA is to be tested further, first for extended bandwidth in the 3kW (electronic warfare) mode, then in the 2kW (phased array radar) mode. Finally the duty factor will be increased for evaluation at full average power. This tube is a good candidate for testing at high average power, since the thermal integrity of the circuit was very good according to measurements made during assembly.

The second tube will be assembled after at least one additional substrate has been photo-etched and laser cut.

4.2 I/J-Band CFA's

Two different options are being pursued in parallel for fabrication of the substrate and meander circuit assembly. One of them incorporates the add-on meander, for which the advantages and disadvantages are well understood. The second is to add a layer of copper foil onto the blank substrate, and then to etch the meander.

One or more cold-test models for a circuit of 0.014" pitch on a substrate 0.006" thick will be completed and tested. These models will use the add-on meander approach. One of the objectives of these cold test models is to establish the input/output RF matching.

Brazed models of the input/output coaxial window assembly are to be built and tested for RF matching.

Parts for three I/J-band tubes are now being fabricated, and these tubes are to be assembled and tested.

APPENDIX

Design Calculations for Meander Circuits*

A.1 Arrays of Bars on Dielectric Supports

The properties of many types of slow-wave structures may be derived from the geometry of an array of parallel bars supported on a dielectric support where the bars are perpendicular to the direction of propagation. The subject considered here is shaped dielectric loading, an example of which is shown in Figure 5, rather than a continuous dielectric support.

An analytical design approach to various slow wave circuits which consist of arrays of bars is presented by the Leblond and Mourier [2]. (Also see Arnaud [3]). This work is based on relating the bar-to-bar and the bar-to-ground capacitances to phase shift per bar and to frequency, taking into account the boundary conditions appropriate to the circuit under consideration (e.g., meander, ladder, interdigital, etc.). No method of predicting these capacitances for shaped dielectrics was presented. Furthermore, no consideration was given to the fact that the phase velocity of a wave is dependent on the proportion of electromagnetic energy falling within the dielectric, which is a function of phase between bars; in most configurations the dielectric between bars is largely space, and the capacitance from a bar to ground is largely in the dielectric medium. The wave is approximated as a TEM wave, a good approximation if dimensions are small compared to a free space wavelength.

* The computer program described here was developed under U.S. Air Force Avionics Laboratory support, Contract No. F33615-79-C-1752.

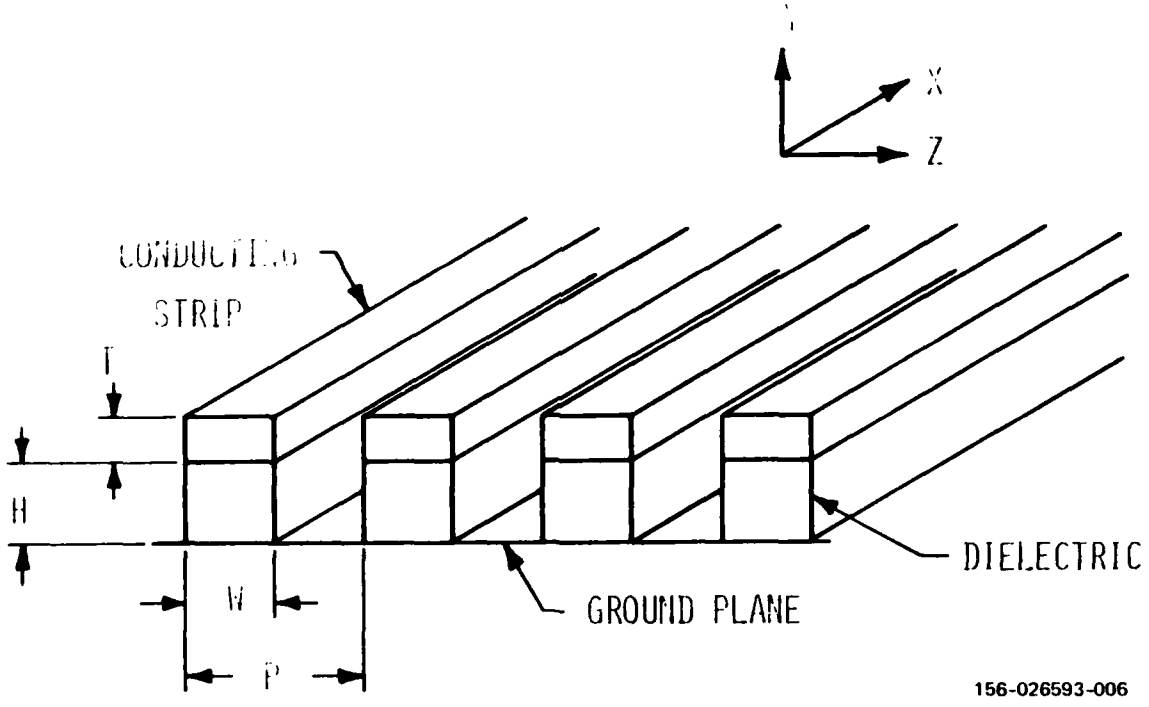

Figure 5. Array of Parallel Conductive Strips Supported on Dielectric Bars.

Analysis of a pair of conducting strips separated from a conducting plane by a continuous dielectric is well known, for example see Bryant and Weiss [4]. Weiss extended this work further to consider an array of thin strips, and by appropriate boundary conditions applied this analysis to a meander [5]. Weiss does take into account that the velocity of propagation along the strips (with a TEM approximation) is dependent on phase difference between bars, as was also done for the analysis of pairs of strips on a dielectric. A propagating wave solution in the dielectric and in space on the side of the circuit away from the ground plane is found. This method of solution is well suited for a thin circuit and continuous dielectric.

The method of analysis described here is based on a static field analysis of the fields between bars, to determine the equivalent capacitance per unit length when each bar of the array is at the same RF potential, and also when adjacent bars are 180° out of phase. The assumed configuration for computer modeling is shown in Figure 6. Only half of one bar is considered, with the right-hand and left-hand boundary conditions established from symmetry.

For the zero mode, the potential of the conducting strip is set equal to 1.0 and that of the ground plane to 0. There is essentially no field above the conductive strip, and therefore surface C is fixed at potential 1.0. Surfaces A, B, and D are by symmetry Neumann boundaries at which the derivative of the potential normal to the surface is zero.

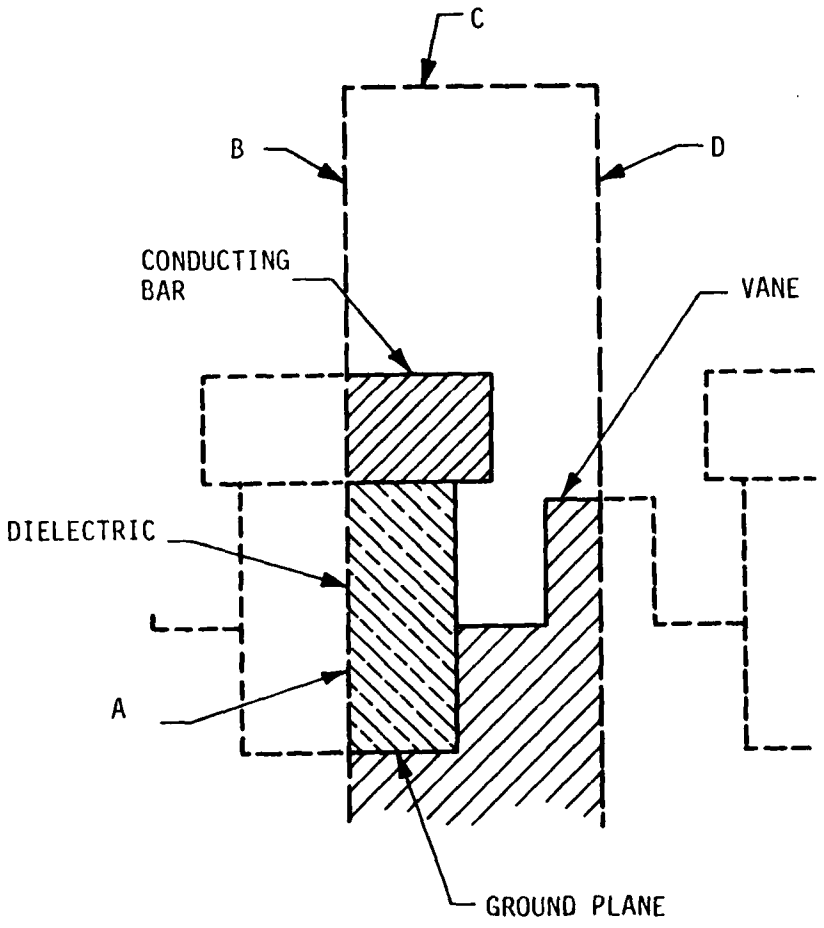

SURFACE	ZERO MODE	PI MODE
BAR	V = 1	V=0 + j1
GROUND	V = 0	V = 0
A	NEUMANN	NEUMANN
B	NEUMANN	NEUMANN
C	V = 1	V = 0
D	NEUMANN	V = 0

$$C_{eff}(\phi) = C_o \cos^2\frac{\phi}{2} + C_{\parallel} \sin^2\frac{\phi}{2}$$

156-026593-008

Figure 6. Half-Pitch Cross Section for Computer Modeling

For the π mode, the conductive strip is set at potential 0 + jl, and each adjacent strip will be at potential 0 - jl. Surface D is at a potential of 0 by symmetry. Surface C is also set at a potential of 0, and is located far enough away from the conductive strip that its effect on the field near the circuit is negligible. In the cylindrical case C is the axis for both modes.

The conventional difference equations, in either rectangular or cylindrical coordinates and with appropriate variation of the mesh parameters at the dielectric boundaries, are solved by the Liebmann method [6]. For simplification of the program, all boundaries lie on mesh points.

Capacitance, C, is calculated from electric energy, U_E, where:

$$U_E = 1/2\ \varepsilon_o \int\int\int \varepsilon_r E^2\ dx\ dy\ dz.$$
$$U_E = 1/2\ CV^2 \qquad (1)$$

Normalized capacitance per unit length, C_n, is given by the following, remembering that V = 1:

$$C_n = \int\int \varepsilon_r E^2\ dy\ dz \qquad (2)$$

The capacitance calculated on the half-bar basis must be doubled to determine the actual capacitance per bar. The effective dielectric constant is determined by repeating the solution with the dielectric material replaced by space but with the other boundary conditions the same (cf. Weiss [4]). The effective dielectric constant is the ratio of the capacitance determined from the first solution to that from the latter. For the zero mode, let C_0 be the capacitance calculated with the dielectric present, and C_{0u} be the capacitance without the dielectric material. The effective dielectric constant for the zero mode is: $\varepsilon_o = C_0/C_{0u}$. If C_π and $C_{\pi u}$ are corresponding values for the π mode, the effective relative dielectric

constant for the π mode is: $\varepsilon_\pi = C_\pi / C_{\pi u}$.

For intermediate values of phase shift, the capacitance per unit length per bar is determined from linear combinations of these capacitance values. The potential from bar to ground is cos $(\phi/2)$ + j sin $(\phi/2)$. The effective capacitance is given by:

$$C_{eff}(\phi) = C_o \cos^2(\phi/2) + C_\pi \sin^2(\phi/2) \qquad (3)$$

The effective dielectric constant is:

$$\varepsilon_{eff}(\phi) = \frac{C_o \cos^2(\phi/2) + C_\pi \sin^2(\phi/2)}{C_{ou} \cos^2(\phi/2) + C_{\pi u} \sin^2(\phi/2)} \qquad (4)$$

The characteristic impedance along a bar is given by:

$$Z_o(\phi) = 377/\sqrt{\varepsilon_{eff}(\phi)}/C_n(\phi) \qquad (5)$$

where $C_n(\phi)$ is a normalized value, equal to actual capacitance per unit length divided by the permittivity of space. The velocity of propagation is equal to $C/\sqrt{\varepsilon_{eff}(\phi)}$ where $\varepsilon_{eff}(\phi)$ is the relative dielectric constant.

A.2 Meander Circuits

The general method of analysis of bar lines described by Leblond and Mourier [2] has been applied specifically to the meander circuit by Sobotka [7]. The dispersion relationship is given by:

$$\tan^2(\phi/2) = \tan^2(kA/2) \quad \frac{\gamma_o + 4\gamma_1 \sin^2(\phi/2) + 4\gamma_2 \cos^2(2\phi/2)\ldots}{\gamma_o + 4\gamma_1 \cos^2(\phi/2) + 4\gamma_2 \cos^2(2\phi/2)\ldots} \qquad (6)$$

In the above, k is the propagation constant along each bar, A is the length of each bar, γ_o is the capacitance from each bar to ground, γ_1 is the capacitance from each bar to the adjacent bar (including only that electric flux directly between the bars), γ_2 is the capacitance from each bar to the

second adjacent, etc. It is assumed that the connections from bar to bar at the ends have zero impedance. The values of γ_2, γ_3, etc. are in practice negligible. Applying the present analysis, $\gamma_0 = C_0$, and it may be shown that $\gamma_0 + 4\gamma_1 = C_\pi$. This solution requires that the propagation velocity along the bars be independent of phase.

To determine a solution for the meander line, Weiss [4] defines even and odd mode quantities according to:

$$\varepsilon_{even} = \varepsilon(\phi); \quad \varepsilon_{odd} = \varepsilon(\phi + \pi)$$

$$k_{even} = (\omega/c)\sqrt{\varepsilon_{even}}; \quad k_{odd} = (\omega/c)\sqrt{\varepsilon_{odd}}$$

$$Z_{even} = Z_0(\phi); \quad Z_{odd} = Z_0(\phi + \pi)$$

As with Sobotka, Weiss assumes short circuits at the ends of the bars. The dispersion law for forward waves is then given by:

$$\tan^2 \frac{\phi}{2} = \frac{Z_{odd}}{Z_{even}} \tan (k_{even}A/2)\tan(k_{odd}A/2) \qquad (7)$$

It may be shown that if $\varepsilon_{even} = \varepsilon_{odd}$, if $C_\pi = \gamma_0 + 4\gamma_1$, and if γ_2, γ_3, etc. are neglected, the above expression is equivalent to (6).

In either method of analysis, the coupling impedance, equal to $|E|^2/2\beta^2 p$, is determined from the stored energy and group velocity. The propagating energy per unit length, W, is easily calculated from the effective capacitance. Power, P, is equal to Wv_g, where v_g, the group velocity is found from the slope of the dispersion curve. The E-field has been assumed constant between bars, and little change is made in the results by integrating the computed E-field.

A typical meander line circuit is shown in Figure 7. Vanes project upward between bars to decrease the ratio of γ_1 to γ_0 (in Sobotka's notation), or to make C_0 more nearly equal to C_π and therefore to make Z_{odd} and k_{odd} more nearly equal to Z_{even} and k_{even} in Weiss's notation. Calculated dispersion curves for a representative meander circuit of such a design are shown in Figure 8, using the dispersion equations of both Sobotka and Weiss. Also shown are two representative experimental curves. It was necessary to choose k, the propagation constant along the bars, arbitrarily for the Sobotka equation as equal to $(\omega/c)(\sqrt{\varepsilon_0}+\sqrt{\varepsilon_\pi})/2$, a value which gives a good fit to experimental results.

At certain frequencies, expression (7) may be negative on the right side. This represents a stop band which is always observed in meander circuits in the neighborhood of $\phi = \pi$. Figure 9 shows an ω - β plot for a meander circuit, observed and calculated from equation (7). The observed stop band is greater than that calculated. This is attributed to the finite impedances at the ends of the bars, which would cause a stop band even if k_{even} and k_{odd} were equal.

Figure 10 compares observed and calculated coupling impedance for the same circuit as in the dispersion curves of Figure 8.

If the electric fields are known, the corresponding magnetic fields and therefore the current distribution on the bars and ground plane can be used to calculate RF losses. The RF loss, W, per unit width, of a mesh element, $\Delta\chi$, is given by:

$$\Delta W = \frac{1}{2} J^2 R_S \Delta\chi$$

where J is the peak value of current density and R_S is the surface re-

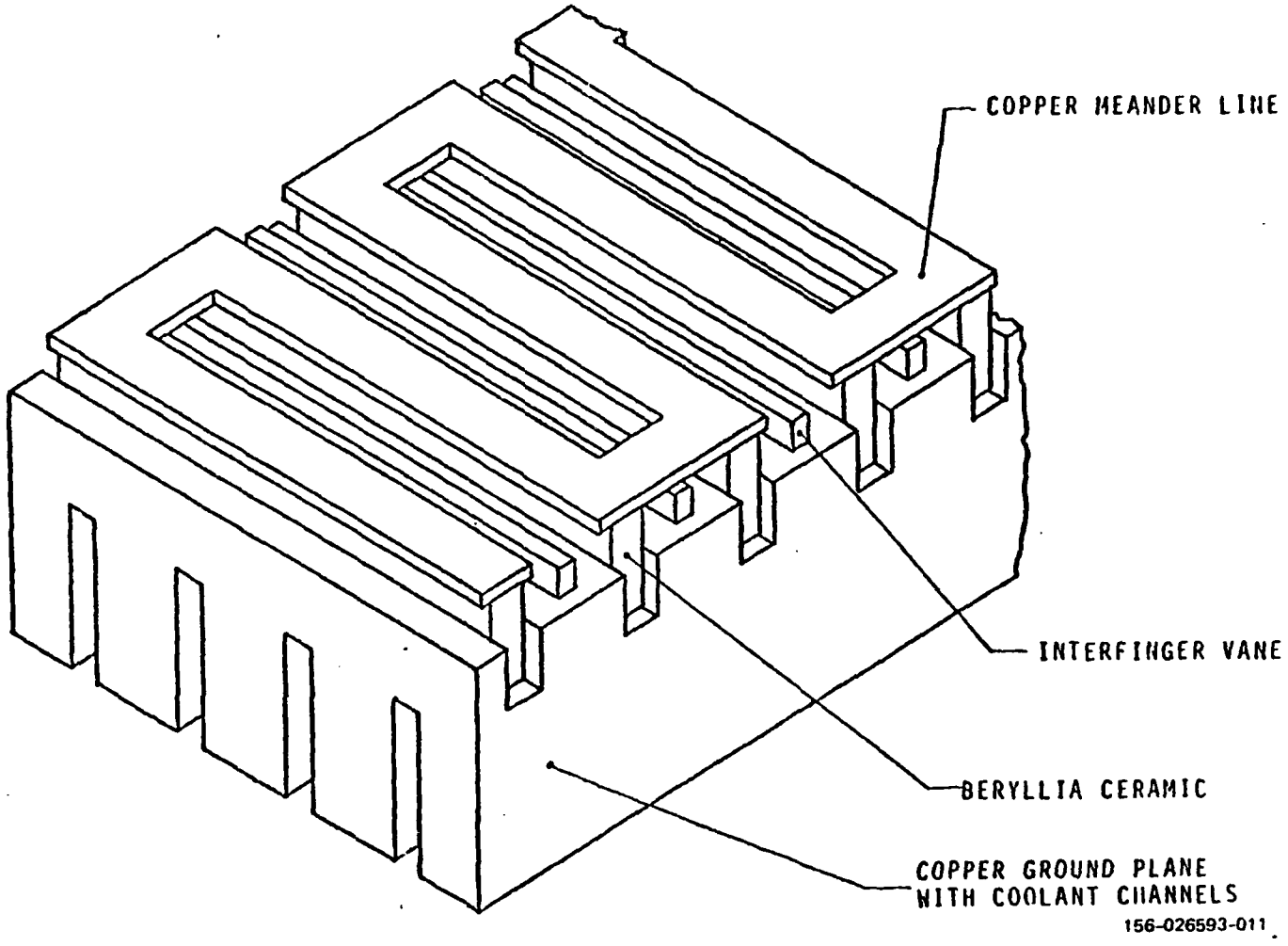

Figure 7. Meander Line (Vane Configuration Indicated)

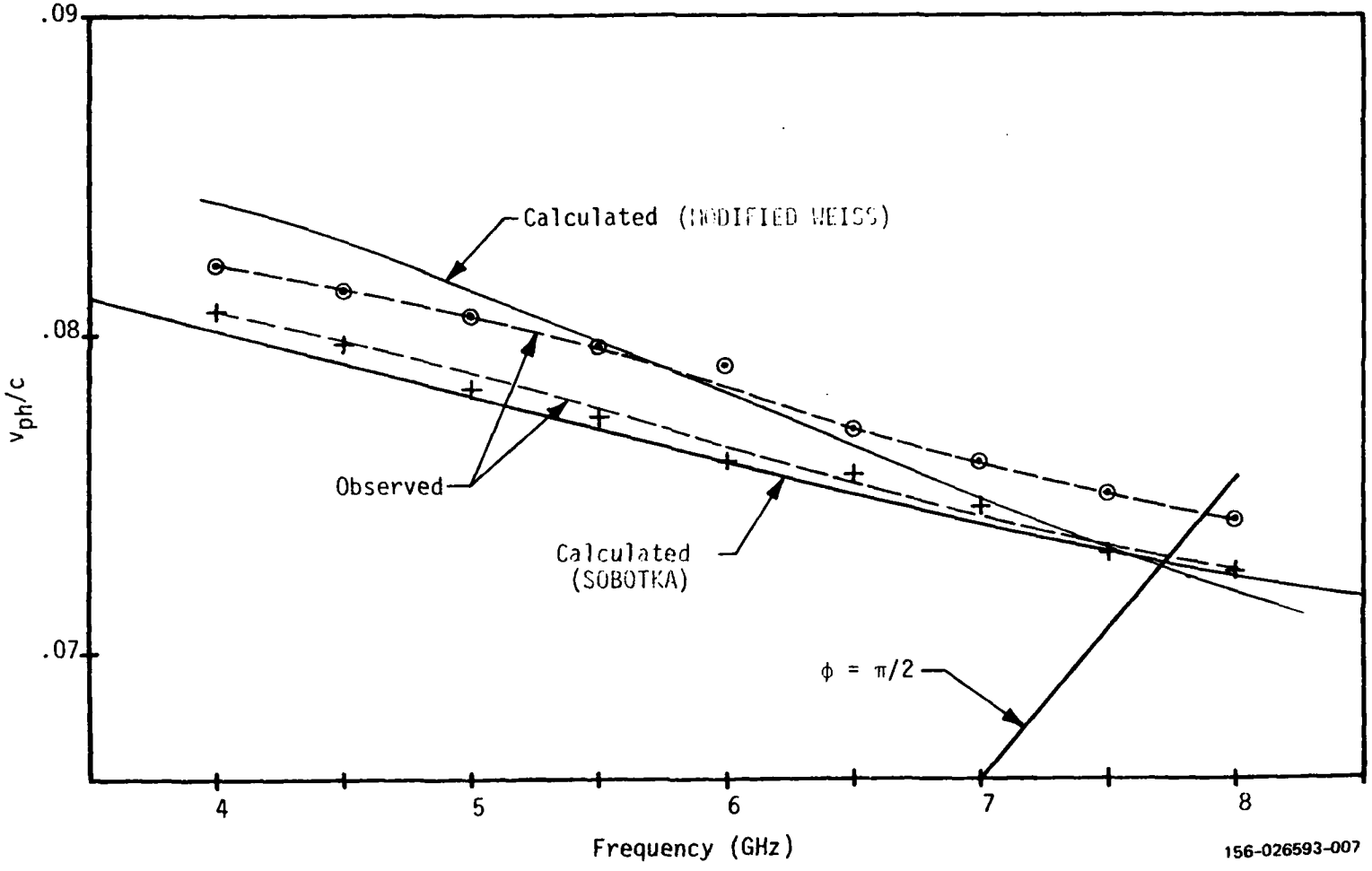

Figure 8. Phase Velocity vs. Frequency of Meander Line

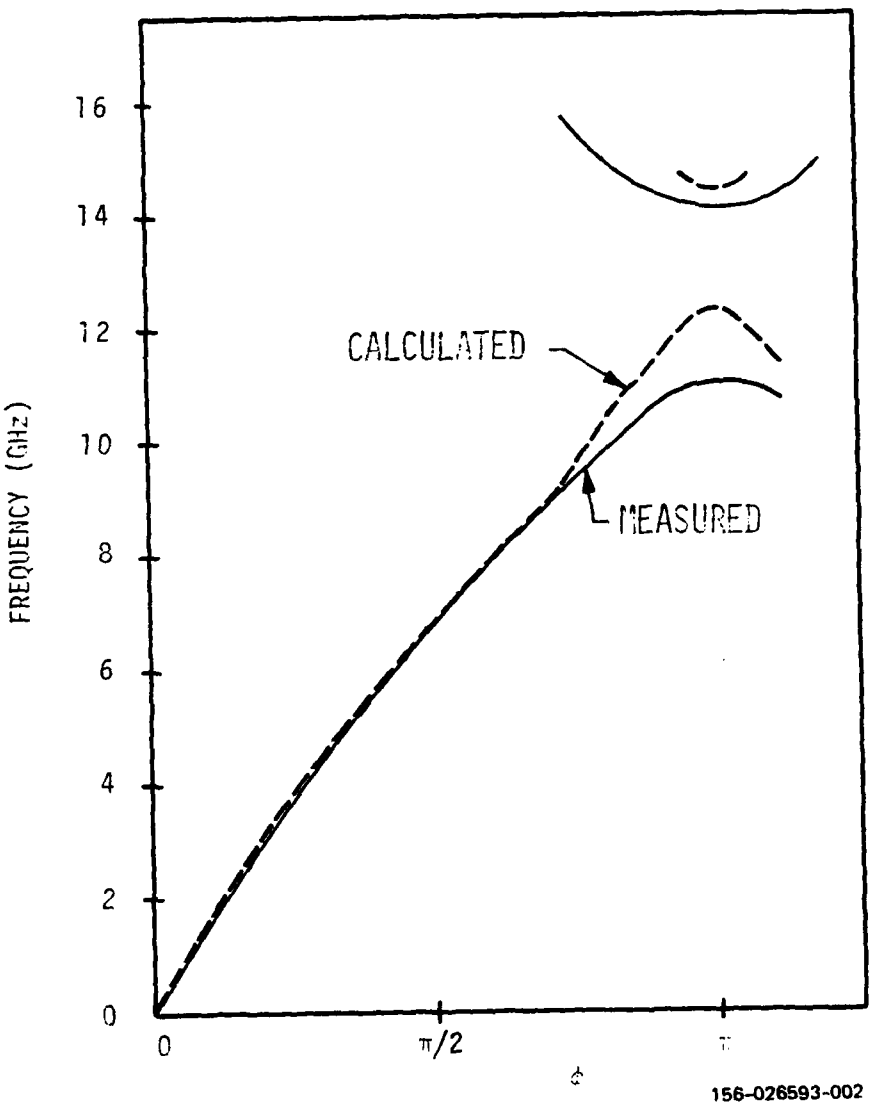

Figure 9. Frequency vs. Phase Shift per Bar of Meander Line

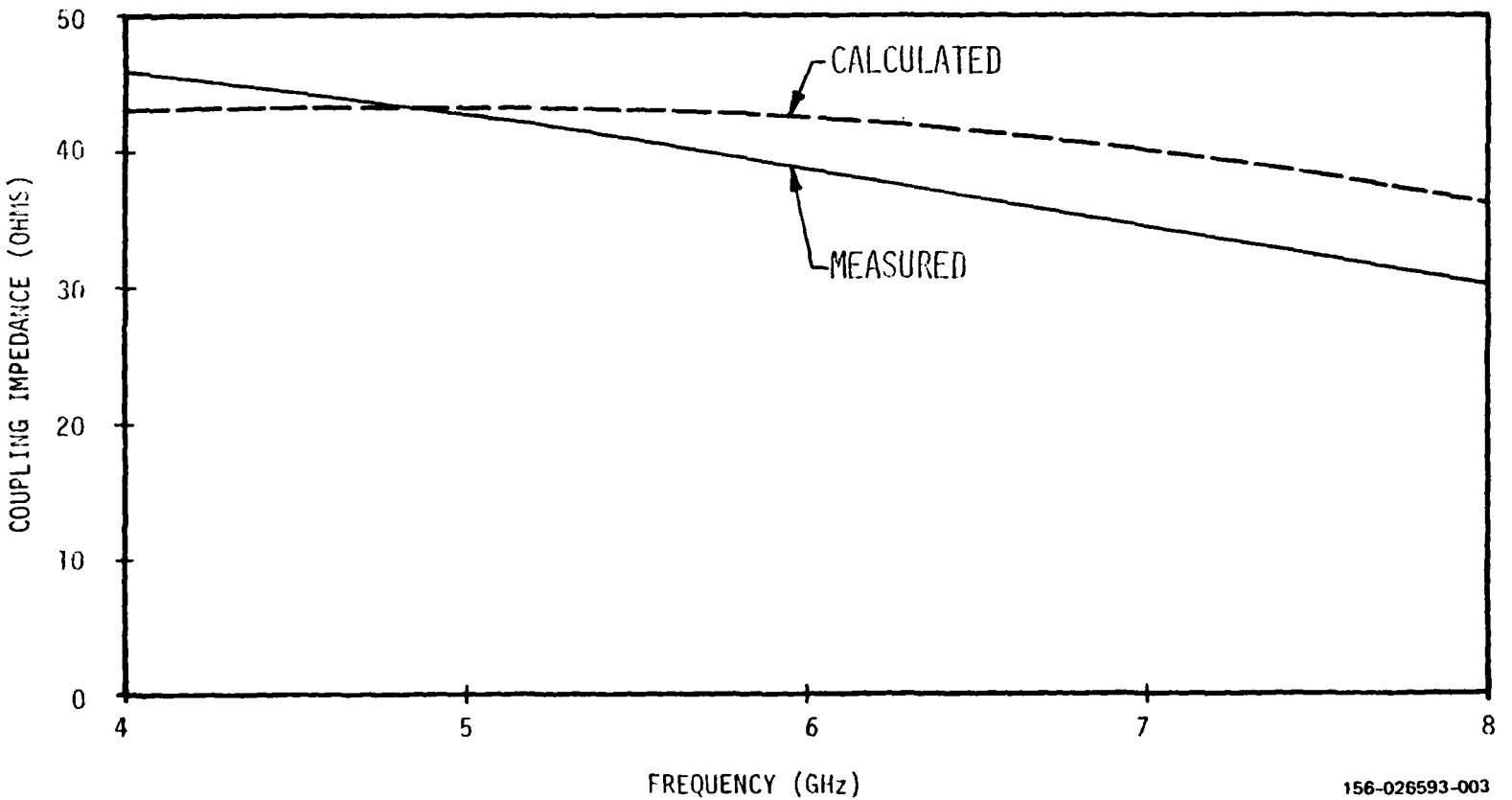

Figure 10. Coupling Impedance of Meander Line at the Level of the Circuit

sistance. Over most surfaces, the surface resistivity is simply that of copper at the frequency of interest. On the metallized surfaces, where the metallizing layer is Ti-Mo-Cu, the effect of the thin layer of molybdenum is taken into account. Figure 11 shows the calculated results for tubes of the same design as in Figures 9 and 10, with two different thicknesses of molybdenum in the metallized layer. Measured attenuation for three representative samples of tubes is also plotted.

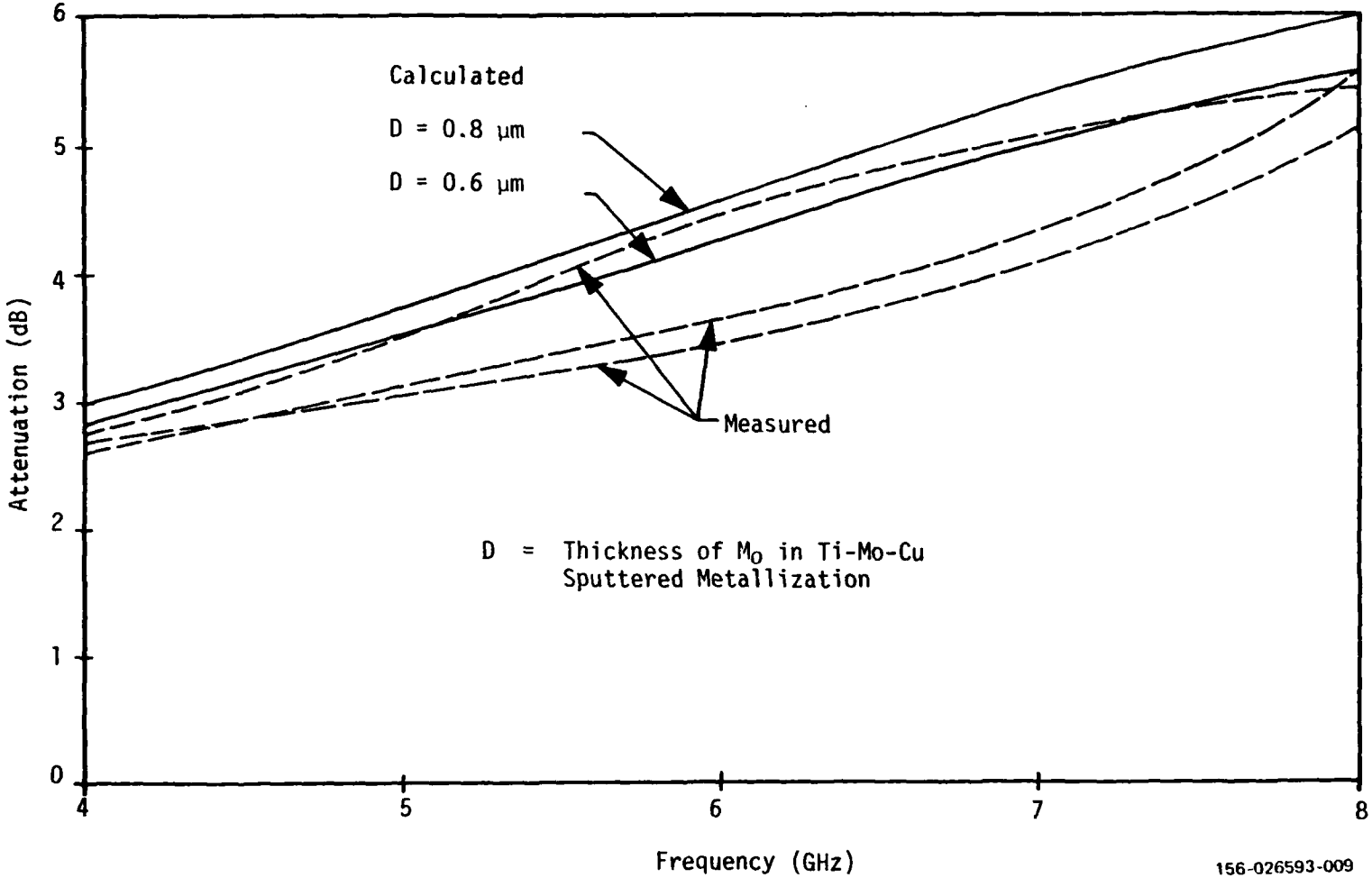

Figure 11. Attenuation of Meander Line

REFERENCES

[1] Research and Development Technical Report No. ECOM-TR-77-2642-3, I/J-Band Crossed-Field Amplifier, Final Technical Report, April 1979.

[2] A. Leblond, G. Mourier, Ann. Radioelectricite, v. 9, p. 311, 1954.

[3] J. Arnaud "Theory of bar lines", Sec 2.2, vol. 1, Crossed-Field Microwave Devices (E. Okress, ed) Academic Press, New York, 1961.

[4] T. Bryant, J. Weiss, "Parameters of Microstrip Transmission Lines and of Coupled Pairs of Microstrip Lines," IEEE Transactions on Microwave Theory and Techniques, vol. MTT-16, pp. 1021-1027, Dec. 1968

[5] J. Weiss "Dispersion and Field Analysis of a Microstrip Meander-Line Slow Wave Structure", IEEE Transactions on Microwave Theory and Techniques, vol. MTT-22, pp. 1194-1201. Dec. 1974.

[6] See, for example, D. McCracken, W. Dorn, Numerical Methods and Fortran Programming, John Wiley and Sons, Inc., New York, 1964

[7] W. Sobotka, Thesis, University of Paris, 1970.

DISTRIBUTION LIST

Agency	Number of Copies
Defense Technical Information Center ATTN: DDC-TCA Cameron Station (Bldg 5) Alexandria, VA 22314	12
Defense Communications Agency Technical Library Center Code 205 (P.A. Tolovi) Washington, DC 20305	1
Code 123, Tech Library DCA/Defense Comm Engring Ctr 1860 Wiehle Ave. Reston, VA 22090	1
Office of Naval Research Code 427 Arlington, VA 22217	1
Director Naval Research Laboratory ATTN: Code 2627 Washington, DC 20375	1
Commander Naval Electronics Lab Center ATTN: Library San Diego, CA 92152	1
Commander US Naval Surface Weapons Center White Oak Laboratory ATTN: Library, Code WX-21 Silver Springs, Md 20910	1
Commander US Army Missile Command ATTN: DRSMI-RD (Mr. Pittman) Redstone Arsenal, AL 35809	1
Deputy for Science & Technology Office, Assist Sec Army (R&D) Washington, DC 20310	1

DISTRIBUTION LIST (Continued)

Agency	Number of Copies
Director US Army Material Systems Analysis Actn ATTN: DRXSY-MP Aberdeen Proving Grounds, MD 21005	1
Commander US Army Logistics Center ATTN: ATCL-MC Fort Lee, VA 22801	2
Cdr. Harry Diamond Laboratories ATTN: Library 2800 Powder Mill Road Adelphi, MD 20783	1
Commander HQ, Fort Huachuca ATTN: Technical Reference Div Fort Huachuca, AZ 85613	1
Cdr. US Army Research Office ATTN: DRXRO-IP PO Box 12211 Research Triangle Park, NC 27709	1
Director US Army Signals Warfare Lab ATTN: DELSW-OS Vint Hill Farms Station Warrenton, VA 22186	1
Commander US Army Nuclear Agency Fort Bliss, TX 79916	1
Commander US Army Satellite Comm Agency ATTN: DRCPM-SC-3 Fort Monmouth, NJ 07703	1
TRI-TAC Office ATTN: TT-SE Fort Monmouth, NJ 07703	1
HQ, US Marine Corps ATTN: Code INTS Washington, DC 20380	1

DISTRIBUTION LIST (Continued)

Agency	Number of Copies
Commander, AVRADCOM ATTN: DRSAV-E PO Box 209 St. Louis MO 63166	1
Commander US Army Electronics R&D Command Fort Monmouth, NJ 07703	
DELEW-D	1
DELCS-D	3
DELAS-D	1
DELET-DD	3
DELET-DT (Mr. J. Teti)	2
DELET-BM (Mr. C. Bates)	22
DELET-BM (Ofc of Record)	1
DELET-P	1
DELSD-L (Tech Library)	1
DELET-D	1
DELET-B (Mr. I. Reingold)	1
DELET-BM (Mr. N. Wilson)	1
DELET-BS (Mr. G. Taylor)	1
DELET-BG (Mr. J. Creedon)	1
DELEW-P (Mr. R. Giordano)	1
DELSD-L-S	2
MIT - Lincoln Laboratory ATTN: Library - Rm A-082 POB 73 Lexington, MA 02173	2
NASA Scientific & Tech Info Facility Baltimore/Washington Intl Airport PO Box 8757, MD 21240	1
Commander US Army Communications R&D Command Fort Monmouth, NJ 07703	
DRDCO-COM-RO	1
USMC-LNO	1
ATFE-LO-EC	1

DISTRIBUTION LIST (Continued)

Agency	Number of Copies
Commander US Army Communications & Electronics Material Readiness Command	
DRSEL-PL-ST	1
DRSEL-MA-MP	1
DRSEL-PP-I-PI	1
DRSEL-PA	2
Advisory Group on Electron Devices 201 Varick St., 9th Floor New York, NY 10014	2
Metals and Ceramics Info Center Batelle 505 King Avenue Columbus, OH 43201	1
DCASMA, Chicago O'Hare Int'l Airport PO Box 66911 ATTN: H. Barcikowski DCRI-GCPE Chicago, IL 60666	1
General Electric Co. Electronics Park Library Bldg Electronics Park ATTN: Yolanda Burke, Doc Librarian Syracuse, NY 13201	1
Hughes Aircraft Co. Mail Station 3255 PO Box 3310 ATTN: Mr. Kalson Fullerton, CA 92634	1
Relmag Div, EEV Inc. 1240 Highway One ATTN: Mr. D. Blank Watsonville, CA 95076	1
Raytheon Company Microwave and Power Tubes Div Foundry Avenue ATTN: Mr. J. Skowron Waltham, MA 02154	1

DISTRIBUTION LIST (Continued)

Agency	Number of Copies
Varian Eastern Tube Div Salem Road ATTN: Dr. G. Farney Beverly, MA 01915	1
Varian Eastern Tube Div Salem Road ATTN: H. McDowell Beverly, MA 01915	1
Litton Industries 1035 Westminster Dr. ATTN: Mr. J. Munger Williamsport, PA 17701	1
Ballistic Missile Defense Advanced Technology Center PO Box 1500 ATTN: RDMH-D (D. Schenk) Huntsville, AL 35807	1
Naval Electronic Laboratory Ctr 271 Catalina Blvd ATTN: J. H. Maynard, Code 2300 San Diego, CA 92152	1
Commander, AFAL ATTN: AFAL/DHM, Mr. W. Fritz Wright-Patterson AFB, OH 45433	1
Litton Industries 960 Industrial Road ATTN: Dr. J.R.M Vaughan San Carlos, CA 94070	1
Microwave Associates South Avenue ATTN: Dr. J. Saloom Burlington, MA 01803	1
Watkins-Johnson Co. 3333 Hillview Ave. Palo Alto, CA 94304	1
ITT Electron Tube Div PO Box 100 Easton, PA 18042	1

DISTRIBUTION LIST (Continued)

Agency	Number of Copies
Rome Air Development Center ATTN: Documents Library (TILD) Griffiss AFB, NY 13441	1
AFGL/SuLL S-29 HAFB, MA 01731	1
HQ, Air Force Systems Command ATTN: DLCA Andrews AFB Washington, DC 20331	1
HQDA (DAMA-ARZ-D/Dr. F. D. Verderame) Washington, DC 20310	1
Commander, DARCOM ATTN: DRCDE 5001 Eisenhower Ave Alexandria, VA 22333	1
Cdr. MIRADCOM Redstone Scientific Info Center ATTN: Chief, Document Section Redstone Arsenal, AL 35809	1
Director, Night Vision & Electro-Optics Lab ATTN: DELNV-D Fort Belvoir, VA 22060	1
Director, Ballistic Missile Defense Advanced Technology Center ATTN: ATC-R, PO Box 1500 Huntsville, AL 35807	1
Chief, Ofc of Missile Electronic Warfare Electronic Warfare Lab, ERADCOM White Sands Missile Range, NM 88002	2
Chief Intel Material Dev & Support Ofc Electronic Warfare Lab, ERADCOM Fort Meade MD 20755	1